ChemistrySelect

Research Article
doi.org/10.1002/slct.202404909

Chemistry Europe
European Chemical Societies Publishing

www.chemistryselect.org

Synthesis and Characterization of Chitosan–Silver Nanocomposite Film: Antibacterial and Cytotoxicity Study

Shephrah Olubusola Ogungbesan,*[a] Eduardo Buxaderas,[b, c] Rosemary Anwuli Adedokun,[d] Yanina Moglie,[b, c, e] Santiago Grijalvo,[f] María Teresa García,[g] Cui Bingbing,[a] David Díaz Díaz,*[b, e] and Guodong Fu*[a]

This study is aimed at the in situ preparation and antibacterial study of silver nanoparticles within the matrix of an eco-friendly, biocompatible, biodegradable, and bioavailable biopolymer (chitosan) to form Chi–AgNP film via multiple non-covalent interactions between the organic polymer and the nanoparticles. The film is fully characterized by infrared and ultraviolet spectroscopy, scanning electron microscopy, transmission electron microscopy, X-ray photoelectron spectroscopy, and thermogravimetric analysis. The characterization confirms the successful incorporation of silver nanoparticles into the polymeric network. Infrared spectroscopy reveals peaks corresponding to the vibration of functional groups present in chitosan with enhanced intensity and blueshifts caused by the presence of silver nanoparticles. Well-monodispersed spherical silver nanoparticles with an average size of 10 nm are observed in the Chi–AgNP film. The surface plasmon resonance at 447 nm is consistent with a typical silver plasmon. Furthermore, the antibacterial effects on *E. coli* and *S. aureus* were determined and attributed to the release of AgNPs observed by UV absorption.

1. Introduction

Pathogenic infections and diseases arising from bacteria have continued to remain a global challenge despite the myriad of available antibiotics. The emergence of antimicrobial resistance through the formation of biofilms further exacerbates these challenges.[1] A biofilm is an assemblage of microbial cells residing within a self-produced extracellular polymeric matrix attached to a living organism. These films have the ability to protect the microbial community from external stresses.[2] These biofilms discharge into the human body, thereby causing chronic infections. It has been estimated that biofilms are responsible for 65% of nosocomial infections, approximately 80% of chronic infections, and 60% of human bacterial infections.[3] The development of biofilms involves four stages. These include the attachment of bacteria cells to the surface of a biomaterial, the adhesion of the cell to the surface, the maturation stage, which involves the formation of a microcolony matrix, and finally, the dispersion of the microcolony. One strategy for tackling these biofilm infections is to develop novel antibacterial films and drug delivery systems for the controlled release of antibiotics.[3,4]

Currently, silver-containing nanocomposite films are receiving considerable attention for use in antimicrobial coatings, patches, plasters, and medication encapsulation. The antimicrobial property of silver has been known for several decades. However, owing to its toxicity, only a few decades ago did exploration intensify its use in antimicrobial activities.[5] However, the manipulation of silver at the nanoscale makes it nontoxic to humans and improves its antimicrobial activity.[6] Silver nanoparticles (AgNPs) can interact with the cell surface of a broad spectrum of microorganisms to cause cytotoxic effects against both Gram-positive and Gram-negative pathogens.[7] The cytotoxic effect increases with decreasing AgNP particle size as smaller particles have an increased ability to penetrate the cell membrane;[8] however, this will not be part of our study. Although the mechanism of action of AgNPs is unclear, it has been suggested that the antibacterial activity of AgNPs hinges on their ability to release silver ions, thereby leading to the for-

[a] S. O. Ogungbesan, C. Bingbing, G. Fu
School of Chemistry and Chemical Engineering, Southeast University, 2 Southeast University Road, Nanjing 211189, P. R. China
E-mail: 233189910@seu.edu.cn
fu7352@seu.edu.cn

[b] E. Buxaderas, Y. Moglie, D. Díaz Díaz
Instituto Universitario de Bio-Orgánica Antonio González, Astrofísico Francisco Sánchez 2, La Laguna, Tenerife 38206, Spain
E-mail: ddiazdiaz@ull.edu.es

[c] E. Buxaderas, Y. Moglie
Instituto de Química del Sur, INQUISUR (CONICET-UNS), Departamento de Química, Universidad Nacional del Sur, Av. Alem 1253, Bahia Blanca 8000, Argentina

[d] R. A. Adedokun
Department of Chemistry, Chrisland University, KM 3, Ajebo Road after FMC, Abeokuta 23409, Nigeria

[e] Y. Moglie, D. Díaz Díaz
Departamento de Química Orgánica, Universidad de La Laguna, Avda. Astrofísico Francisco Sánchez 3, La Laguna, Tenerife 38206, Spain

[f] S. Grijalvo
CIBER-BBN, ISCII. Jordi Girona 18–26, 0, Barcelona 8034, Spain

[g] M. T. García
Department of Surfactants and Nanobiotechnology, Institute of Advanced Chemistry of Catalonia (IQAC-CSIC), Barcelona 08035, Spain

Supporting information for this article is available on the WWW under https://doi.org/10.1002/10.1002/slct.202404909

mation of free radicals and reactive oxygen species that inhibit deoxyribonucleic acid replication. These features of AgNPs make them excellent candidates for antibacterial and antimicrobial applications in various medical and industrial settings.[1a,6d,9] Despite the unique properties of antibiotics against drug-resistant pathogens, stabilization is usually needed, and in this regard, biopolymers have gained considerable attention as stabilizing agents. Furthermore, stabilization with biopolymers further reduces AgNP toxicity and increases bioavailability.[1a]

Chitosan, a biopolymer formed from the deacetylation of chitin, is one of the most preferred stabilizing agents. This stems from its biodegradable, bioavailable, biocompatible, and mucoadhesive properties.[10] In addition, its drug encapsulation ability, gradual burst release, drug efficiency modification, release rate regulation, and therapeutic selectivity improvement have attracted much research attention, and its use in diagnostic tools, food packaging, animal food production, targeted drug delivery systems, and drug encapsulation has been limited.[11] Chitosan, in the form of nanoparticles, nanofibers, nanosponges, nanoscaffolds, nanocomposite film, nanogels, nanocapsules, and hydrogels, has been used to improve drug stability, solubility, therapeutic, and pharmacokinetic properties.[12] Chitosan is a cationic linear polyaminosaccharide composed of poly[β-(1–4)-linked-2-amino-2-deoxy-d-glucose]. The manipulation and functionalization of chitosan molecules with different functional groups can involve physical or chemical processes such as grafting, crosslinking complexation, and polymer doping.[13] Equally advantageous is that chitosan also serves as reducing and stabilizing agent in the reduction of silver substrates to AgNPs,[14] leading to a greener protocol compared to the ones reported in the literature where the use of other reducing agents is conventional.[15] The incorporation of AgNPs through multiple noncovalent interactions into the polymeric matrix of chitosan to form Chi–AgNP film will provide a nontoxic material with an efficient drug delivery system for the sustained release of antimicrobial agents capable of penetrating biofilms and microbial cells responsible for antibiotic resistance.[16]

Herein, we describe the in situ preparation, characterization, antibacterial, and cytotoxic activities of stable silver nanoparticle-embedded chitosan (Chi–AgNP) films. The fabrication of films of the Chi–AgNP in such films may prevent drug degradation during storage or during blood circulation compared to other formats such as bulk gels,[14] solid particles,[17] or liquid formulations.[18] Preliminary data regarding the release dynamics of these materials are also included in our study.

2. Experimental Section

2.1. Materials

Chitosan with a degree of deacetylation $\geq$95%, 100–200 (mPa·s), sodium hydroxide (NaOH), silver nitrate ($AgNO_3$), buffer solutions pH 7 and pH 4, acetic acid, and all other reagents were purchased from Shanghai Aladdin Biochemical Technology Co. Ltd. All reagents were of analytical grade and were used as received from the supplier. Double-distilled water was used in the preparation of all aqueous solutions. *E. coli* (DH5α), *S. aureus* (ATCC 25,923), U-937 cells, human skin fibroblast, lysogeny broth (LB), and Mueller–Hinton agar (MHA) were purchased from BeyoClick™, China.

2.2. Preparation of Chitosan Film (Chi Film)

Chitosan film was prepared following the known casting and solvent evaporation methods.[19] First, 1.2 g of chitosan was dissolved in 100 mL of 0.175 M glacial acetic acid. The mixture was vigorously stirred at room temperature for 3 h to obtain a clear transparent slurry, which was cast on a glass petri dish for even contact. The excess slurry was poured off the petri dish, and the well-coated petri dish was placed in a vacuum dryer (Electrothermal Blast Drying Oven PS-9040BS model) and allowed to dry at 35 °C for 3 h. To harvest the film, the petri dish was soaked in 0.01 M NaOH solution for 60 s, washed with double-distilled water three times until the medium became pH 6.89, and carefully removed from the petri dish. The harvested film was thereafter dried and stored for characterization, in vitro release, and bacterial inhibitory studies.

2.3. Preparation of Chitosan–Silver Nanoparticles Film (Chi–AgNP Film)

The Chi–AgNP film was prepared by dissolving 0.6 g of chitosan in 50 mL of 0.175 M glacial acetic acid. The mixture was vigorously stirred at room temperature until a clear transparent slurry was formed. This was followed by the addition of 20 mL of 0.0589 M $AgNO_3$ solution, and the mixture was stirred for 6 h during which the slurry gradually turned blackish brown, indicating the formation of silver nanoparticles. The slurry was subsequently cast into a petri dish and dried. The dried film was soaked in 0.01 M NaOH solution for 60 s, washed with double-distilled water three times until the medium became pH 6.89, before final drying and storage, as in the preparation of the chitosan film.

2.4. Material Characterization

Fourier transform infrared (FTIR) spectroscopy was used to identify the presence of functional groups. Vacuum-dried samples of Chi film and Chi–AgNP film were evenly combined with KBr powder at a ratio of 1:100, ground, and then compressed to 10 tons to create pellets. The disc containing the prepared pellet was then placed inside FTIR spectrometer (Nicolet 8700 American Nancorporation) disc holder. One hundred scans were performed on the samples to obtain a transmission spectrum at a 4 cm^{-1} spectral resolution in the mid-infrared region from 4000 to 400 cm^{-1}.

The morphology was determined using high-resolution transmission electron microscopy (Talos F200X). The samples were dispersed in acetic acid (0.5%). The suspension was ultrasonicated for 10 min, the mixture was dotted on a TEM grid and left to incubate for 5 min after which the excess sample on the grid was removed. The grid was then allowed to air dry. Later, the grid was placed in the sample holder, and the sample holder was carefully placed in the transmission electron microscope.

The surface morphology and elemental analysis of Chi film and Chi–AgNP film were determined using field emission scanning electron microscopy with energy-dispersive x-ray (SEM–EDX) (FEI Inspect F50 American Nancorporation).

The particle scattering, size distribution and average size of the particles were ascertained via dynamic light scattering (DLS) on a Brookhaven's nanoparticle size and zeta potential analyzer.

X-ray photoelectron spectroscopy (XPS) studies of Chi–AgNP film was performed using an AXIS HIS 165 spectrometer (Kratos Analytical, Manchester, UK) with a monochromatic Al Kα X-ray source (1486.71 eV photons). A Shirley background type was employed for the XPS fitting, and the carbon deposit peak at 284.7 eV served as the reference calibration standard. The XPS chamber vacuum was 10^{-9} mbar.

UV–visible absorption spectra of the Chi film and Chi–AgNP film were recorded at wavelengths ranging from 200 to 800 nm using an UV–visible spectrophotometer (UV 2600) (Shimadzu Corporation, Japan).

Thermogravimetric analysis (TGA) was conducted utilizing a NETZSCH TG 209F3A apparatus in a nitrogen environment with a heating rate of 10 °C/min and a scanning range spanning from 30 to 960 °C.

The swelling of films was assessed in phosphate-buffered saline (PBS) solution at pH 7.4. First, 0.0089 g of Chi film and 0.0041 g of Chi–AgNP film were immersed in PBS for several hours. After that, the films were removed from the solution and the mass of the films were obtained after careful removal of the excess of water from the surface of the films.

The swelling ratio of each film was calculated at each time interval using the formula below:

$$\text{Swelling Ratio} = \frac{\text{weight per time} - \text{initial weight}}{\text{initial weight}} \times 100 \quad (1)$$

2.5. In Vitro Antibacterial Activity Study

The sample solution was first prepared at a concentration of 1 mg/mL and subsequently diluted to 50 and 25 µg/mL in 96-well plates and sterilized with UV light. Next, 100 µL of bacterial suspension was added to each well of a 96-well plate, containing different concentrations of sample solution, to obtain final concentration as 10^6 CFU/mL of *E. coli* or 10^7 CFU/mL of *S. aureus*, after which the mixture was mixed well. The optical density of each well was measured at 600 nm with a microplate reader. The microplates were then placed in a biochemical incubator and incubated for 24 h. Finally, after this period of time, the optical density (OD) value of each well was measured at 600 nm.

The minimum inhibitory concentration (MIC) was calculated using the Equation (2):

$$\text{MIC} = \frac{\Delta\,(\text{OD}) - \Delta'\,(\text{OD})}{\Delta\,(\text{OD})} \quad (2)$$

where Δ(OD) is the increase of the optical density in the blank control group and Δ'(OD) is the increase of the optical density value of the different samples after 24 h of incubation.

Mueller-Hinton (MH) agar plates were used to cultivate *S. aureus*, whereas Luria-Bertani (LB) agar plates were used to cultivate *E. coli*.

2.6. Cytotoxicity Test

A human skin fibroblast suspension (5×10^4 cells/mL) were seeded in a 96-well plate and incubated at 37 °C in a 5% CO_2. After 24 h, samples (Amoxil, Chi film, and Chi–AgNPs) were prepared to a final concentration of 500 µg/mL and sterilized by UV light. The prepared sample solutions (100 µL) were added to a 96-well plate and incubated in the presence of cells for an additional 24 h. Untreated cells incubated with only 100 µL of 1 × PBS were used as the blank control. Next, 10 µL of CCK-8 solution was added to the above mixture, which was subsequently incubated at 37 °C for 1 h. The OD at 450 nm was subsequently measured using a microplate reader (Infinite F50, Tecan, Switzerland).

The cell viability rate was calculated using the Equation (3).

$$\text{Cell viability rate\%} = \frac{\text{d}'\,(\text{OD})}{\text{d}\,(\text{OD})} \times 100 \quad (3)$$

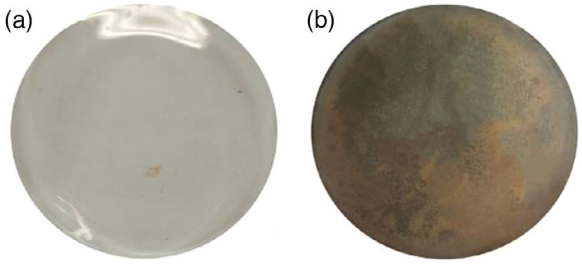

Figure 1. a) Formation of AgNPs in the slurry after 10 min of slurry casting. b) Harvested fully populated Chi–AgNP film.

2.7. Statistical Analysis

OriginPro 8.5 was used to statistically examine the data received from each analysis, which was carried out in triplicate. The findings were presented in the manner of mean. Using Duncan's multiple range tests and one-way analysis of variance (ANOVA), the mean significant differences between treatments were computed. A significance threshold of $p < 0.05$ was applied.

3. Results and Discussion

3.1. Preparation of Chitosan–Silver Nanoparticles Film (Chi–AgNP film)

During preparation of the Chi–AgNP film, the mixture was first transparent, but after one hour of stirring, it became brown, indicating the in situ formation of silver nanoparticles inside the chitosan matrix (Figure 1). As acetic-acid-activated chitosan was the only reducing agent present in the mixture, chitosan demonstrated an effective reducing capacity.[20] The mechanism for the formation of the chitosan–silver nanocomposite film involves the activation of the amine sites of chitosan by protonation using diluted glacial acetic acid. The silver atoms could then attach to each monomer of chitosan through the amine group. The formation of chitosan-capped silver nanoparticles is achieved after the reduction of silver ions through the amino group. The same amino group of chitosan also coordinates with the pH-based controlled release of the metal ion.[21]

3.2. Characterization of Film and Nanocomposite

3.2.1. FTIR Analyses

The FTIR spectra showed the vibrational frequencies of the absorbing functional groups present in the Chi-film and Chi–

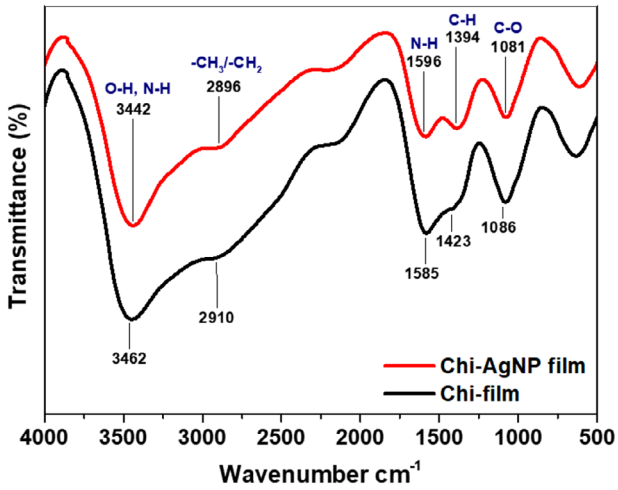

Figure 2. FTIR spectra of Chi film and Chi–AgNP film.

AgNP film (Figure 2). The spectrum of the Chi-film showed a strong peak at 3462 cm^{-1} that was suspected to be a result of OH/NH band stretching in chitosan. The weak peak appearing at 2910 cm^{-1} was assigned to aliphatic CH_2/CH_3 groups in the Chi-film. The band at 1585 cm^{-1} matched the bending vibration of the NH_2, and the signals at 1423 and 1086 cm^{-1} were attributed to C—N and C—O—C bands. The introduction of silver nanoparticles into the chitosan matrix led to a broadening of the OH/NH bands, with a shift from 3462 to 3442 cm^{-1} due to hydrogen bonding and a shift in the aliphatic CH_2/CH_3 band from 2910 to 2896 cm^{-1}. Moreover, the bending vibration of the NH_2 band suffered a slight blueshift from 1585 to 1596 cm^{-1}, whereas the C—N band was shifted from 1423 to 1394 cm^{-1}, and the C—O—C band suffered a tiny shift from 1086 to 1081 cm^{-1}.

3.2.2. TEM, SEM, and EDX Analyses

TEM observed well-defined spherical silver nanoparticles, with a particle size distribution of ca. 10.0 ± 1.5 nm (Figure 3a). The particle size of the chitosan–silver nanocomposite synthesized in this study was smaller than that reported in Kalaivani et al.,[22] but larger than that reported by Gowda and Sriram.[23] The selected area electron diffraction (SAED) pattern of Chi–AgNP film is shown in Figure 3b. The corresponding (111), (200), (220), (311), and (420) lattice planes indicate the formation of crystalline silver nanoparticles in the synthesized Chi–AgNP film.[24] SEM analysis (Figure 3c,d) shows the surface morphology of Chi film and Chi–AgNP films. The micrograph showing the surface morphology of silver nanocomposite film was quite similar to the micrographs obtained by Susilowati et al., Gowda and Sriram, and Pan et al.[20,23,25] These authors prepared chitosan–silver nanoparticles using chemical reduction, electrodeposition, and chemical reduction assisted by microwave irradiation. The SEM micrograph, which was in agreement with the TEM results, showed that the particles were spherical. The surface of Chi–AgNP film was relatively homogenous, suggesting that the silver nanoparticles were uniformly dispersed within the chitosan matrix.

The elemental composition determined by EDX showed a distinct peak for silver, indicating that the silver was well dispersed in the chitosan polymeric matrix (Figure 4a). The absorption signal at approximately 3 keV indicated the presence of silver nanoparticles.[26] Other peaks, which included those of C and O, were attributed to the presence of chitosan surrounding the silver nanoparticles.[23] Figure 4c–e shows the peak maps for the distributions of Ag, C, and O.

3.2.3. DLS Analyses

The particle size distribution of the Chi–AgNP film is shown in Figure 5. DLS analysis revealed that the mean hydrodynamic diameter of silver nanocomposite was 113.48 nm. Compared to that of the TEM analysis, the DLS revealed a larger particle size because DLS measures the hydrodynamic diameter of the hydrated polymer shell. The polydispersity index (PDI) for this nanocomposite was 0.206. A PDI less than 0.4 suggests that the Chi–AgNP film was fairly monodispersed.[1a]

3.2.4. XPS Analyses

XPS was used to determine the valence states of silver nanocomposite and the chemical makeup of the products. The survey-scan XPS spectra of Chi–AgNP film (Figure 6a–d) showed that the sample was composed of silver (368.83 and 374.87 eV), nitrogen, with one peak at 399.70 eV; oxygen, with two peaks (528.18 and 535.13 eV); and carbon, with three peaks (283.88, 288.41, and 291.54 eV). Figure 6e displays the silver high-resolution XPS result. Two distinct peaks in the Ag 3d XPS signals are linked

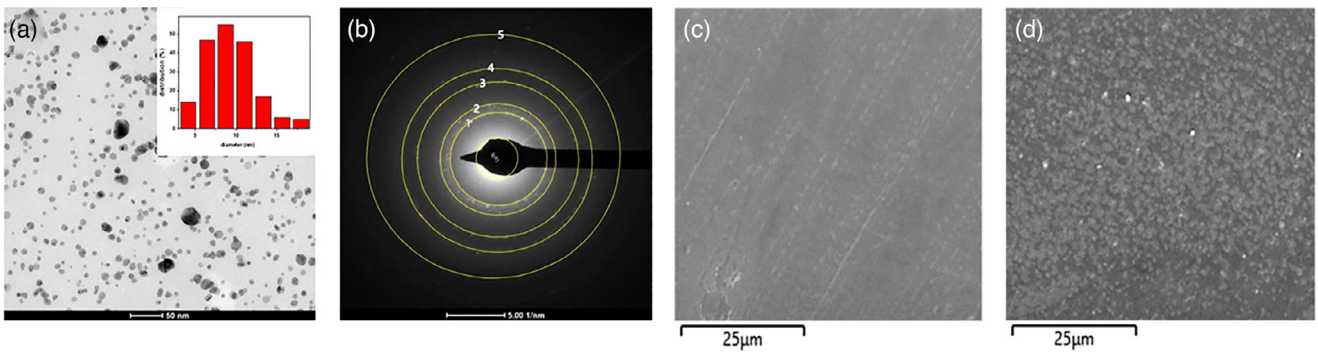

Figure 3. (a) TEM image of Chi–AgNP film. (b) SAED image of Chi–AgNP film. SEM image of (c) pure Chi film and (d) Chi–AgNP film.

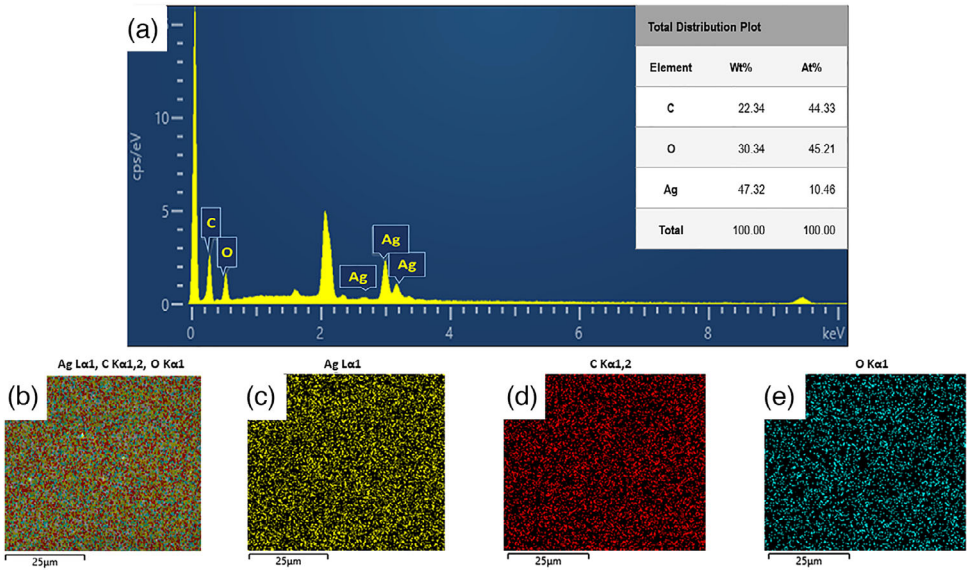

Figure 4. EDX image of Chi–AgNP film.

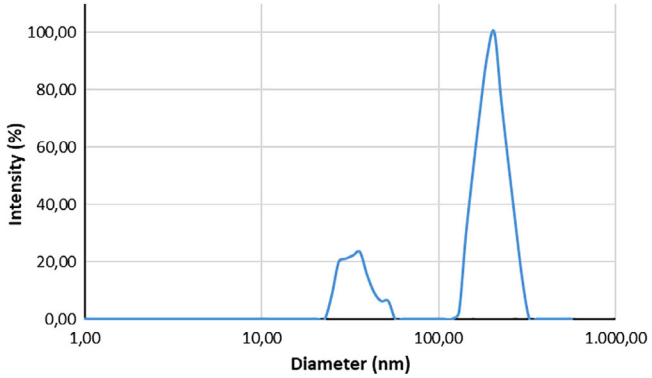

Figure 5. DLS spectrum of Chi–AgNP film.

to the Ag 3d5/2 (368.83 eV) and Ag 3d3/2 (374.87 eV) orbitals. Ag^0 was assigned to the two silver peaks suggesting that the sample consisted of metallic silver, which is consistent with the SAED results displayed in Figure 3b.[27] The XPS results indicate that pure metallic silver was produced throughout the reaction, which supports the notion that chitosan was used as the reducing agent to completely reduce Ag^+ to Ag^0.

3.2.5. UV Analyses

The UV–vis spectra in Figure 7b show that the synthesized Chi–AgNP film has blue-shifted absorption compared to that of bulk silver with a resonance of approximately 1000 nm. The surface plasmon resonance (SPR) band for this nanocomposite film was centered at 446 nm. This finding is consistent with the literature as it has been reported that AgNPs have a surface plasmon resonance within the range of 410–450 nm.[7a,28] The SPR peak at 446 nm further confirmed that spherical particles were formed, as revealed by TEM analysis.[29] The Chi film spectrum shows one absorption peak at 305 nm, which is the π–π* transition (Figure 7a). On the other hand, Chi–AgNP film exhibit two peaks at 268 nm and 446 nm, which signifies successful incorporation of the silver nanoparticles in the polymeric matrix.

Moreover, the Chi film showed a bandgap of 5.85 eV, whereas the bandgap of the Chi–AgNP was 5.35 eV. This decrease in the energy gap means that the material becomes more absorptive in the visible light range (see Supporting Information).

3.2.6. TGA and DTG Analyses

The presence of AgNPs normally enhances the thermal stability of chitosan. TGA thermograms (black line) and DTG analyses (red line) of Chi film and Chi–AgNP film are shown in Figure 8. From 30 to 160 °C, Chi film exhibited a weight loss of 11%, and from approximately 250 °C to 400 °C, another 54% decrease in mass was observed (Figure 8a). In the silver nanocomposite, the first weight loss of approximately 7% is observed between 30 and 100 °C (Figure 8b). The second rapid weight loss began at approximately 220 °C and flattened as the temperature approached 400 °C, for a weight loss of 42%. In both cases, the weight losses can be attributed to the loss of water molecules and amine and CH_2OH, respectively, revealing that most of the organic matter was degraded, leaving more thermally stable AgNPs.[30] The effect of AgNPs on the thermal stability of the nanocomposite is markedly evident as the temperature approaches 250 °C. The total mass loss was 63% and 50% for Chi film and Chi–AgNP film, respectively. This result is consistent with the findings of Hasibuan et al.[7a] The temperatures for maximum weight losses were determined and are clearly presented in the DTG graphs. Chi film decomposition temperature was about 274 °C. The introduction of AgNPs increased the decomposition temperature to 284 °C.

3.2.7. Swelling Analyses

The ability of the synthesized film to swell is crucial to this study because it affects how drugs are released, how wounds heal,

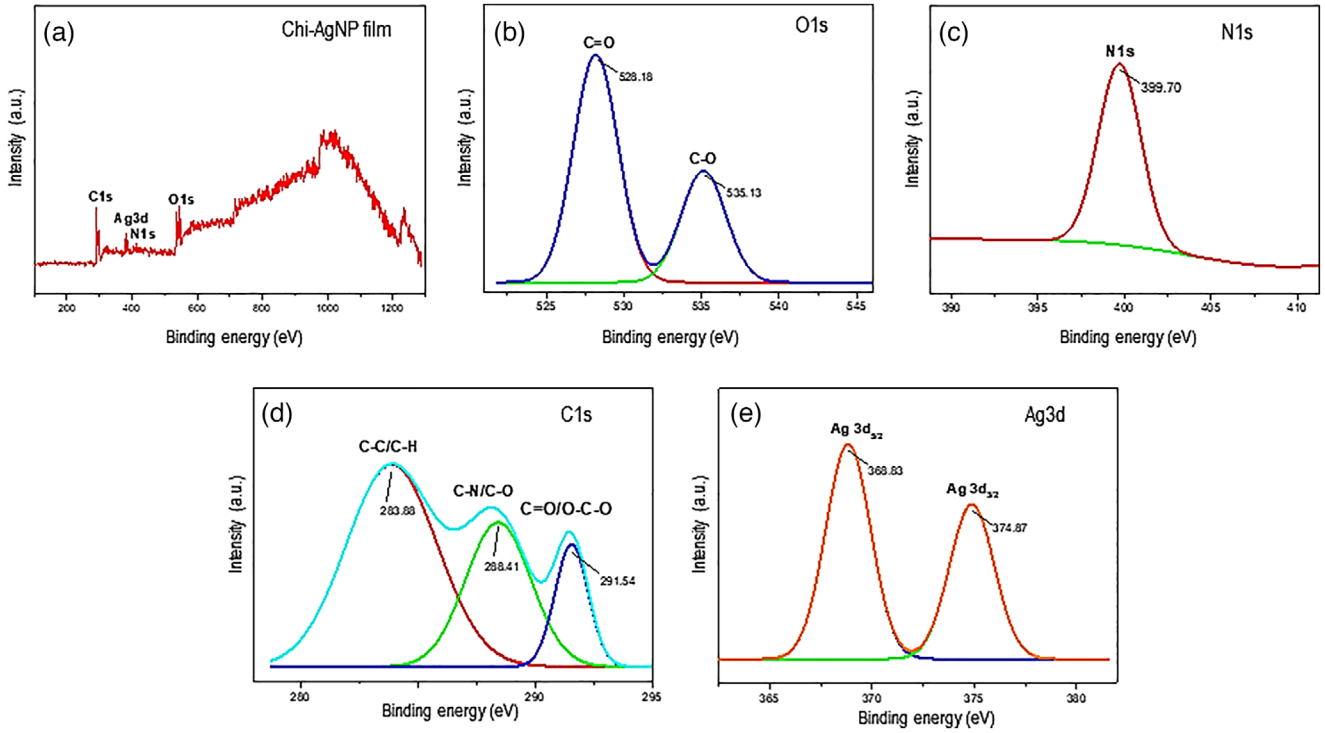

Figure 6. (a) XPS spectrum of Chi–AgNP film. (b) O1s. (c) N1s. (d) C1s and (e) Ag3d.

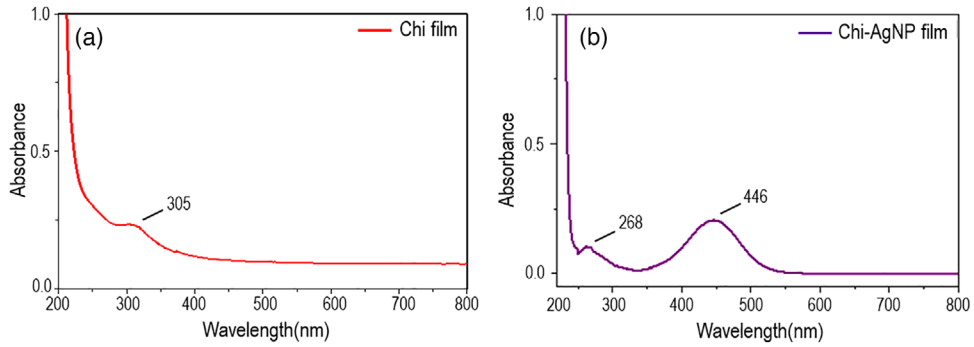

Figure 7. UV–visible spectrum of (a) Chi film and (b) Chi–AgNP film.

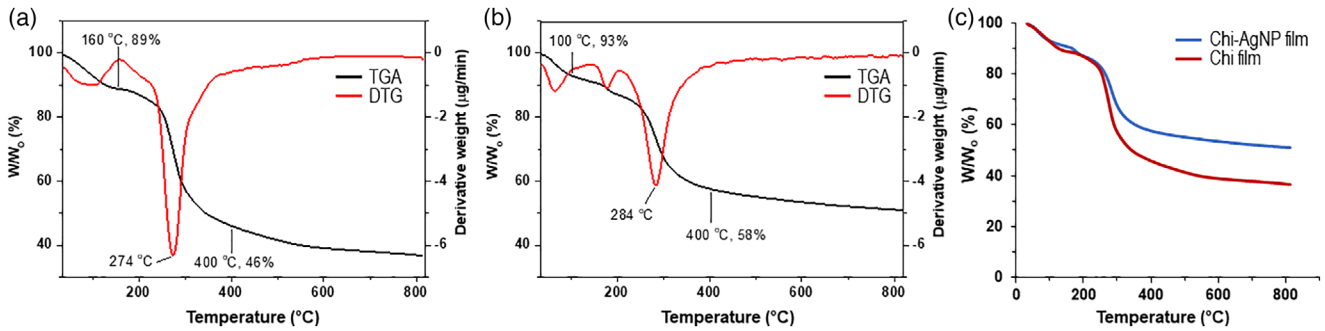

Figure 8. Thermograms of (a) Chi film and (b) Chi–AgNP film. (c) Overlap thermograms of Chi film and Chi–AgNP film.

how antibacterial properties work, and other medicinal applications. The swelling ratios of the prepared Chi film and Chi–AgNP film are displayed in Figure 9. The structural porosity of the chitosan film network explains why the swelling ratio of Chi film was greater than that of Chi–AgNP film. The decreased swelling ratio of Chi–AgNP film could be explained by the attachment of silver nanoparticles to the electron-rich atoms of chitosan and the binding of the nanoparticles to the porous surface of the chi-

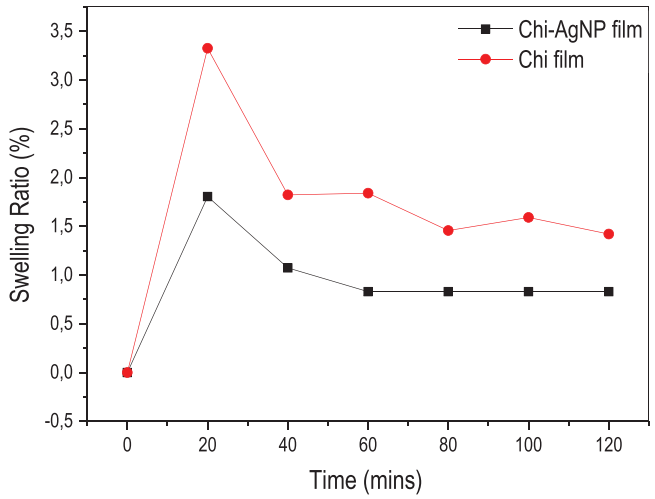

Figure 9. Swelling study of Chi film and Chi–AgNP film.

tosan. As a result, the network develops crosslinks that limit the intake of water.[31]

In addition, the release dynamics of silver nanoparticles in the Chi–AgNP film were preliminary analyzed via UV–visible spectrometry in a qualitative manner (see Supporting Information). The observed trends suggest a controlled and sustained release mechanism. However, further studies are still necessary to demonstrate this point and establish undoubtedly the mechanism and the kinetics. We are currently working on this aspect and the results will be published at due course.

3.3. Evaluation of Biological Activity

3.3.1. Antibacterial Efficacy

Amoxicillin (Amoxil) served as the standard for assessing the antibacterial efficacy of Chi film and Chi–AgNP film against *E. coli* (Figure 10a) and *S. aureus* (Figure 10b). Two distinct concentrations (25 µg/mL and 50 µg/mL) of amoxicillin, Chi film, and Chi–AgNP film were tested in this study.

Amoxil at 25 and 50 µg/mL demonstrated ineffectiveness in inhibiting both test organisms. In contrast, Chi-film and Chi–AgNP film exhibited a concentration-dependent response. At 25 µg/mL, they did not inhibit bacterial growth against *S. aureus* and showed only low inhibitory activity against *E. coli*. In contrast, at 50 µg/mL, there was a marked increase in their biocidal activity. At this concentration, the Chi film demonstrated inhibition values of approximately 60% against both bacterial strains, whereas the Chi–AgNP film exhibited inhibition values close to 100% against *S. aureus* (92%) and completely inhibited bacterial growth against *E. coli* (100%). Therefore, the incorporation of silver nanoparticles into the chitosan film significantly enhances its antibacterial activity.

Notably, the efficiency of the synthesized Chi film and Chi–AgNP film at the observed concentration surpasses that of amoxicillin, a well-known antibiotic in clinical use.

3.3.2. Citotoxicity

Following the confirmation of the quality of our synthesized Chi–AgNP film, we were tasked with evaluating the biological characteristics of Chi–AgNP film. Viability assays are fundamental as they provide insights into cellular responses to toxicants, including metabolic activities. The CCK-8 assay facilitates sensitive colorimetric assessments, which enables the determination of viable cell numbers in cell proliferation processes and cytotoxicity. Figure 11 illustrates the variation in human skin fibroblasts after exposure to 500 µg/mL of Chi–AgNP film for 24 h. Additionally, Chi film, Amoxil, and untreated cells (blank control) were included in this study. As depicted in Figure 11, both Chi and Chi–AgNP film caused a relatively moderate decrease in cell activity with viability percentages of 83.7 ± 7.3% and 71.9 ± 13.5% at the same concentration. The slight variation in the cellular viability produced by Chi and Chi–AgNP film were not statistically significant ($p > 0.05$). Conversely, Amoxil did not produce any effect on the cellular proliferation of skin fibroblasts.

The Chi–AgNP film showed great antibacterial activity at low minimum inhibition concentration in comparison with other related systems found in the literature (see Supporting Information). In addition, the cytotoxicity of the Chi–AgNP film synthesized is significantly lower compared to similar systems in the literature (see Supporting Information).

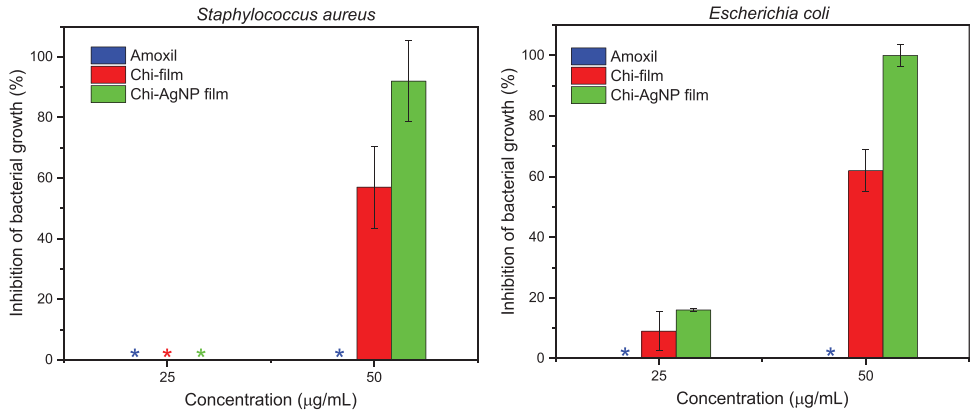

Figure 10. Inhibition of bacterial growth of (a) *S. aureus* and (b) *E. coli* by amoxicillin, Chi film, and Chi–AgNP film.

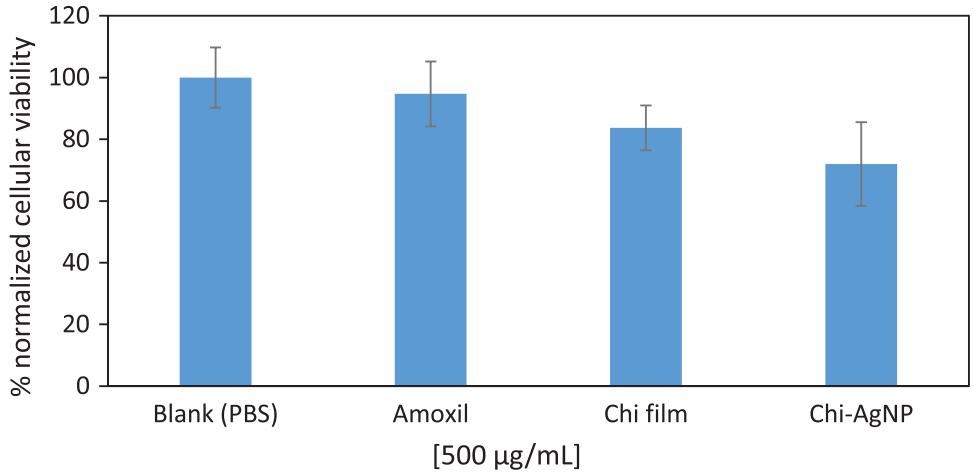

Figure 11. Cytotoxicity of Chi and Chi–AgNP film did not affect human skin fibroblasts according to the CCK-8 assay. Fibroblasts were exposed to Chi and Chi–AgNP film at 500 µg/mL for 24 h. Results are shown as the % of treated cells compared to untreated cells. Data is the average of three independent experiments (SD = 3).

4. Conclusions

Chitosan was used in the synthesis of silver nanoparticle films as a reducing and stabilizing agent. An analysis of the produced films showed that the antibacterial qualities were superior to those of traditional antibiotics. The optimum particle sizes inside the film matrix and the uniform dispersion of silver nanoparticles within the chitosan matrix are responsible for this exceptional efficacy. Additionally, the investigation revealed how silver nanoparticles catalytically degrade chitosan without causing denaturation. This catalytic characteristic highlights the adaptability of nanocomposite films for possible use in controlled deterioration or environmental remediation scenarios. Cytotoxicity evaluations showed that biocompatibility was maintained at greater doses while being at its best at the lowest inhibitory concentration. This shows that nanocomposite films may be used in biomedical applications without having a negative impact on the viability of cells. Preliminary dynamic release data of the nanocomposite films are in agreement with the antibacterial activity observed.

Acknowledgements

This work was supported by the National Natural Science Foundation of China under Grant 52073059. Shephrah Olubusola Ogungbesan thanks Southeast University Scholarship, Nanjing, China, and Nanjing Municipal Government Scholarship, China. Yanina Moglie thanks the Spanish Government for María Zambrano postdoctoral grant. David Díaz Díaz thanks the Spanish Government for the projects: TED2021-132847B-I00/AEI/10.13039/501100011033/ Unión Europea NextGenerationEU/PRTR and PID2022-142118OB-I00/MCIN/AEI/10.13039/501100011033/UE. David Díaz Díaz also thanks NANOtec, INTech, Cabildo de Tenerife and ULL for the laboratory facilities.

Conflict of Interests

The authors declare no conflict of interest.

Data Availability Statement

The data that support the findings of this study are available from the corresponding author upon reasonable request.

Keywords: Antibacterial film · Biopolymers · Chitosan · Silver nanoparticles

[1] a) V. Kulikouskaya, K. Hileuskaya, A. Kraskouski, Y. Kozerozhets, E. Stepanova, I. Kuzminski, L. You, V. Agabekov, *SPE Polymers* **2022**, *3*, 77; b) N. F. Kamaruzzaman, L. P. Tan, K. A. M. Yazid, S. I. Saeed, R. H. Hamdan, S. S. Choong, W. K. Wong, A. Chivu, A. J. Gibson, *Materials* **2018**, *11*, 1705.
[2] a) W. Li, J. Zhang, F. Wang, L. Qian, Y. Zhou, W. Qi, J. Chen, *Chemosphere* **2018**, *202*, 586; b) A. Penesyan, I. T. Paulsen, S. Kjelleberg, M. R. Gillings, *NPJ Biofilms Microbiomes* **2021**, *7*, 80; c) S. Sharma, J. Mohler, S. D. Mahajan, S. A. Schwartz, L. Bruggemann, R. Aalinkeel, *Microorganisms* **2023**, *11*, 1614.
[3] P. Li, R. Yin, J. Cheng, J. Lin, *Int. J. Mol. Sci.* **2023**, *24*, 11680.
[4] a) M. Cloutier, D. Mantovani, F. Rosei, *Trends Biotechnol.* **2015**, *33*, 637; b) H. O. Gbejuade, A. M. Lovering, J. C. Webb, *Acta Orthop.* **2015**, *86*, 147; c) A. N. A. Kamaruzzaman, T. E. T. Z. Mulok, N. H. M. Nor, M. F. Z. R. Yahya, *Malays. Appl. Biol.* **2022**, *51*, 57.
[5] a) M. E. I. Badawy, T. M. R. Lotfy, S. M. S. Shawir, *Bull. Natl. Res. Cent.* **2019**, *43*, 83; b) B. Nowack, H. F. Krug, M. Height, *Environ. Sci. Technol.* **2011**, *45*, 1177.
[6] a) L. F. G. Chabala, C. E. E. Cuartas, M. E. L. López, *Mar. Drugs* **2017**, *15*, 328; b) Z. Su, D. Sun, L. Zhang, M. He, Y. Jiang, B. Millar, P. Douglas, D. Mariotti, P. Maguire, D. Sun, *Materials* **2021**, *14*, 2351; c) I. X. Yin, J. Zhang, I. S. Zhao, M. L. Mei, Q. Li, C. H. Chu, *Int. J. Nanomed.* **2020**, *15*, 2555; d) C. Zanca, S. Carbone, B. Patella, F. Lopresti, G. Aiello, V. Brucato, F. Carfi Pavia, V. La Carrubba, R. Inguanta, *Polymers* **2022**, *14*, 3915.
[7] a) P. A. Z. Hasibuan, Yuandani, M. Tanjung, S. Gea, K. Pasaribu, M. Harahap, Y. A. Perangin-Angin, A. Prayoga, J. G. Ginting, *Heliyon.* **2021**, *7*, e08197; b) E. Hermosilla, M. Díaz, J. Vera, M. J. Contreras, K. Leal, R. Salazar, L. Barrientos, G. Tortella, O. Rubilar, *Int. J. Mol. Sci.* **2023**, *24*, 2318.

[8] a) S. Mumtaz, S. Ali, S. Mumtaz, T. A. Mughal, H. M. Tahir, H. A. Shakir, *Polym. Bull.* **2023**, *80*, 4719; b) M. A. Asghar, R. I. Yousuf, M. H. Shoaib, M. A. Asghar, N. Mumtaz, *BIOI* **2021**, *2*, 71; c) A. M. Shehabeldine, S. S. Salem, O. M. Ali, K. A. Abd-Elsalam, F. M. Elkady, A. H. Hashem, *J. Fungi* **2022**, *8*, 612.
[9] a) J. S. Kim, E. Kuk, K. N. Yu, J.-H. Kim, S. J. Park, H. J. Lee, S. H. Kim, Y. K. Park, C.-Y. Hwang, Y.-K. Kim, Y.-S. Lee, D. H. Jeong, M.-H. Cho, *Nanomedicine* **2007**, *3*, 95; b) I. O. Wulandari, B. E. Pebriatin, V. Valiana, S. Hadisaputra, A. D. Ananto, A. Sabarudin, *Materials* **2022**, *15*, 4641; c) Z. Yu, Q. Li, J. Wang, Y. Yu, Y. Wang, Q. Zhou, P. Li, *Nanoscale Res. Lett.* **2020**, *15*, 115.
[10] a) Y. Yao, M. Xia, H. Wang, G. Li, H. Shen, G. Ji, Q. Meng, Y. Xie, *Eur. J. Pharm. Sci.* **2016**, *91*, 144; b) P. Liu, X. S. Piao, S. W. Kim, L. Wang, Y. B. Shen, H. S. Lee, S. Y. Li, *J. Anim. Sci.* **2008**, *86*, 2609; c) J. H. Park, G. Saravanakumar, K. Kim, I. C. Kwon, *Adv. Drug Delivery Rev.* **2010**, *62*, 28.
[11] a) R. Abdeen, N. Salahuddin, *J. Chem.* **2013**, 576370; b) X. Z. Tang, P. Kumar, S. Alavi, K. P. Sandeep, *Crit. Rev. Food Sci. Nutr.* **2012**, *52*, 426; c) R. Rahmi, M. Marlina, N. Nisfayati, *Orient. J. Chem.* **2017**, *33*, 478.
[12] Y. Herdiana, N. Wathoni, S. Shamsuddin, M. Muchtaridi, *Heliyon.* **2022**, *8*, e08674.
[13] F. Seidi, M. K. Yazdi, M. Jouyandeh, M. Dominic, H. Naeim, M. N. Nezhad, B. Bagheri, S. Habibzadeh, P. Zarrintaj, M. R. Saeb, M. Mozafari, *Int. J. Biol. Macromol.* **2021**, *183*, 1818.
[14] M. Patel, T. Kikani, U. Saren, S. Thakore, *Int. J. Biol. Macromol.* **2024**, *262*, 129968.
[15] a) H. Huang, X. Yang, *Biomacromolecules* **2004**, *5*, 2340; b) M. Potara, A. M. Gabudean, S. Astilean, *J. Phys. Chem.* **2011**, *21*, 3625.
[16] a) P. Ghadam, P. Mohammadi, A. A. Ali, in *Silver Nanomaterials for Agri-Food Applications* (Ed: K. A. Abd-Elsalam), Elsevier, Amsterdam, The Netherlands **2021**, pp. 67–99; b) P. B. da Silva, V. H. S. Araújo, B. Fonseca-Santos, M. C. Solcia, C. M. Ribeiro, I. C. da Silva, R. C. Alves, A. M. Pironi, A. C. L. Silva, F. D. Victorelli, M. A. Fernandes, P. S. Ferreira, G. H. da Silva, F. R. Pavan, M. Chorilli, *Curr. Med. Chem.* **2021**, *28*, 1906.
[17] M. Mondéjar-López, A. J. López-Jimenez, O. Ahrazem, L. Gómez-Gómez, E. Niza, *Int. J. Biol. Macromol.* **2023**, *225*, 964.
[18] G. J. C. Canama, M. C. L. Delco, R. A. Talandron, N. P. Tan, *ACS Omega* **2023**, *8*, 17699.
[19] a) L. Cui, S. Gao, X. Song, L. Huang, H. Dong, J. Liu, F. Chena, S. Yua, *RSC. Adv.* **2018**, *8*, 28433; b) S. M. Riyadh, K. D. Khalil, A. Aljuhani, *Nanomaterials* **2018**, *8*, 928.
[20] E. Susilowati, Maryani, Ashadi, Marwan, *IOP Conf. Ser.: Mater. Sci. Eng.* **2020**, *858*, 012042.
[21] Z. Nate, M. J. Moloto, P. K. Mubiayi, P. N. Sibiya, *MRS Adv.* **2018**, *3*, 2505.
[22] R. Kalaivani, M. Maruthupandy, T. Muneeswaran, A. H. Beevi, M. Anand, C. M. Ramakritinan, A. K. Kumaraguru, *Front. Lab. Med.* **2018**, *2*, 30.
[23] S. Gowda, S. Sriram, *Plant Nano Biol.* **2023**, *5*, 100041.
[24] N. G. Madian, N. Mohammed, *J. Mater. Res. Technol.* **2020**, *9*, 12970.
[25] J. Pan, Z. Zhang, Z. Zhan, Y. Xiong, Y. Wang, K. Cao, Y. Chen, *Carbohydr. Polym.* **2020**, *242*, 116391.
[26] A. Shah, A. A. Ashames, M. A. Buabeid, G. Murtaza, *J. Drug Deliv. Sci. Technol.* **2020**, *55*, 101366.
[27] S. Huang, J. Wang, Y. Zhang, Z. Yu, C. Qi, *Nanomaterials* **2016**, *6*, 118.
[28] C. T. Handoko, N. G. Moustakas, T. Peppel, A. Springer, F. E. Oropeza, A. Huda, M. D. Bustan, B. Yudono, F. Gulo, J. Strunk, *Catalysts* **2019**, *9*, 323.
[29] K. Jyoti, M. Baunthiyal, A. Singh, *J. Radiat. Res. Appl. Sci.* **2016**, *9*, 217.
[30] Y. Estévez-Martínez, R. V. Mora, Y. I. M. Ramírez, E. Chavira-Martínez, R. Huirache-Acuña, J. N. Díaz-de-León-Hernández, L. J. Villarreal-Gómez, *Sci. Rep.* **2023**, *13*, 10234.
[31] K. Vimala, Y. M. Mohan, K. S. Sivudu, K. Varaprasad, S. Ravindra, N. N. Reddy, Y. Padma, B. Sreedhar, K. MohanaRaju, *Colloids Surf. B Biointerfaces* **2009**, *76*, 248.

Manuscript received: October 16, 2024